Accepted Manuscript

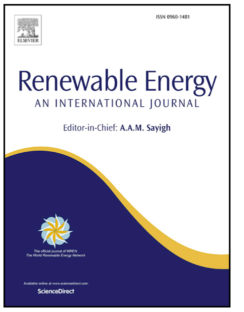

Modelling impacts of tidal stream turbines on surface waves

Xiaorong Li, Ming Li, Stuart McLelland, Laura-Beth Jordan, Laurent Amoudry, Qingyang Song, Andy Plater

PII: S0960-1481(18)30623-2

DOI: 10.1016/j.renene.2018.05.098

Reference: RENE 10150

To appear in: *Renewable Energy*

Received Date: 20 June 2017

Revised Date: 28 May 2018

Accepted Date: 29 May 2018

Please cite this article as: Li X, Li M, McLelland S, Jordan L-B, Amoudry L, Song Q, Plater A, Modelling impacts of tidal stream turbines on surface waves, *Renewable Energy* (2018), doi: 10.1016/j.renene.2018.05.098.

Modelling impacts of tidal stream turbines on surface waves

Xiaorong Li[a,], Ming Li[b], Stuart McLelland[c], Laura-Beth Jordan[c], Laurent Amoudry[d], Qingyang Song[e], Andy Plater[a]

[a]*School of Environmental Sciences, University of Liverpool, Liverpool, L69 7ZT, U.K.*
[b]*School of Engineering, University of Liverpool, Liverpool, L69 3GQ, U.K.*
[c]*School of Environmental Sciences, University of Hull, Cottingham Road, Hull, HU6 7RX*
[d]*National Oceanography Centre, Joseph Proudman Building, 6 Brownlow Street, Liverpool, L3 5DA*
[e]*FTZ-Westkste/Coastal Research Laboratory, Christian-Albrechts-Universitt zu Kiel, Kiel, Germany*

Abstract

A high resolution Computational Flow Dynamics (CFD) numerical model is built based on a laboratory experiment in this research to study impacts of tidal turbines on surface wave dynamics. A reduction of $\sim 3\%$ in wave height is observed under the influence of a standalone turbine located 0.4 m from the free surface. The artificial wave energy dissipation routine 'OBSTACLE' within FVCOM is shown to effectively capture the correct level of wave height reduction, reproducing the CFD results with significantly less computational effort.

The turbine simulation system is then applied to a series of test cases to investigate impact of a standalone turbine on bed shear stress. Results suggest an apparent increase in bed stress ($\sim 7\%$) upstream of the turbine due to the inclusion of surface waves. However, in the immediate wake of the turbine, bed stress is dominated by the presence of the turbine itself, accounting for a $\sim 50\%$ increase, with waves having a seemingly negligible effect up to 9D downstream of the turbine. Beyond this point, the effect of waves on bed shear stress become apparent again. The influence of OBSTACLE on bed stress is also noticeable in the far wake, showing a reduction of $\sim 2\%$ in wave height.

Keywords: Tidal stream energy, Oceanographic model, Wave-current coupling, Bottom shear stress

Nomenclature

$\bar{P}$	The time-averaged static pressure
$\bar{u}_i$ $(\bar{u}, \bar{v}, \bar{w})$	The time-averaged water velocities in the x_i (x, y, z) directions
δ_{ij}	The Kronecker delta
μ	The molecular viscosity
ρ	The water density
σ	The relative frequency
θ	The wave direction
$\vec{C}_g$	The group velocity vector
$\vec{V}$	The ambient water current vector
C_σ	The wave propagation velocity in frequency space
C_θ	The wave propagation velocity in directional space

c_d The drag coefficient

c_L The lift coefficient

d The water depth

f The Coriolis parameter

f_d The drag force

F_i The external body forces in the i directions (x, y, z)

f_L The lift force

F_u The horizontal momentum term in the x direction

F_v The horizontal momentum term in the y direction

H The wave height

K_m The vertical eddy viscosity coefficient

K_t The wave energy transmission coefficient of OBSTACLE

L The wave length

N The wave action density spectrum

N_b The number of blades

P_a The air pressure at sea surface

P_H The hydrostatic pressure

q The non-hydrostatic pressure

S_{tot} The source-sink terms

t Time

u The velocity component in the x direction

U_r The Ursell number

v The velocity component in the y direction

V_{tot} The fluid velocity relative to the blade

w The velocity component in the z direction

x The east axis in the Cartesian coordinate system

y The north axis in the Cartesian coordinate system

z The vertical axis in the Cartesian coordinate system

u'_i (u', v', w') The fluctuating water velocities in the x_i (x, y, z) directions

BBL The Bottom Boundary Layer module

BEM The Blade Element Method

CFD Computational Flow Dynamics

FVCOM The Unstructured Grid Finite Volume Community Ocean Model

HATT Horizontal Axis Tidal Turbine

RANS The Reynolds-averaged Navier-Stokes equations

ROMS Regional Ocean Modelling System

SWAN Simulating Waves Nearshore

TbM (BBL) A TbM case with bottom shear stress calcuated through BBL, otherwise bottom shear stress is calcuated through Equations described in section 2

TNO Wave-current FVCOM case without obstacle (for model verification)

TNO15 Wave-current FVCOM case without obstacle (for impact identification)

TSR Tip Speed Ratio

TYO Wave-current FVCOM case with obstacle activated at the turbine location (for model verification)

TYO15 Wave-current FVCOM case with obstacle activated at the turbine location (for impact identification)

VBM The Virtual Blade Model

VOF The Volume of Fluid method

1. Introduction

As a very promising clean, non-carbon alternative to traditional fossil fuels, tidal stream energy has been gaining significant attention. However, despite the growing interest in this sector of renewable energy, our understanding of the impacts of tidal stream energy devices on the surrounding environment is still limited, largely due to the lack of data collected from on-site projects.

Alternatively, laboratory experiments and numerical simulations are widely adopted to investigate such impacts. For example, porous actuator disc simulators [1, 2, 3] and down-scaled turbine prototype models [4, 5] have been used in laboratories to study turbine-caused impacts on passing flows and turbulence. Also, [6] carried out laboratory experiments to study changes of wake recovery of a turbine subjected to opposing waves. As a complement to laboratory experiments, Computational Flow Dynamics (CFD) modelling is also commonly applied. Similarly, works with turbines approximated as porous discs [7, 8, 9] and with realistic turbine geometry resolved in the computational mesh [10, 11, 12] have been published to reveal how flow patterns and turbulent mixing are changed by the turbine in near-field scale.

To study the far-field hydrodynamic changes caused by the operation of turbines and turbine arrays, numerical oceanographic models, such as Regional Ocean Modelling System (ROMS) [13] and The Unstructured Grid Finite Volume Community Ocean Model (FVCOM) [14], have also been used. Modifications have been made to such models in order to simulate the effect of tidal stream turbines on the flow motion. These modifications are mostly based on either the additional bottom friction approach [15, 16, 17] or the turbine-induced body force concept [18, 19, 20, 21, 22, 23, 24].

In an effort to account for turbine-caused impacts on turbulence in large scale oceanographic models, [25] added three terms to the $k-\epsilon$ closure within ROMS to model turbine related turbulence generation, dissipation and turbulence length-scale interference. These three terms were later adapted accordingly to accommodate the theory around which the MY-2.5 turbulence closure is based and applied in FVCOM by [26].

In terms of interactions between surface waves and tidal turbines, current research focus has been mainly put on the impact of waves on the performance of turbines due to its immediate industry relevance [27, 28, 29, 30, 31, 32, 33]. However, there is a lack of emphasis on the effects of turbines on surface waves in both physical experimental studies and numerical modelling. Because tidal turbines are normally expected to be installed in relatively shallow coastal waters due to difficulties in device installation and operation that would occur otherwise [2], they are likely to have a close proximity to the free surface and hence interfere with the propagation of surface waves. Also, the altered three-dimensional flow structure due to the presence of tidal turbines could also have influence on surface waves through wave-current interaction mechanisms. Surface waves, particularly in shallow coastal areas, can influence sediment transport dynamics significantly. For instance, vertical mixing in the water column due to wave activities can keep sediment in suspension for longer, inhibiting sediment deposition in the downstream areas of the turbine [34]. Also, wave actions can increase bottom shear stress, leading to enhanced sediment resuspension and erosion [35]. Further, through wave-current interactions, waves can drive longshore currents, contributing to long-term shoreline evolution [36, 37]. Therefore, changes in wave dynamics caused by tidal turbines are of high importance in terms of fully understanding impact of tidal turbines on local and regional geomorphology.

Due to the aforementioned interactions, the primary objectives of the work documented in this paper are to first explore the potential impacts of tidal turbines on surface waves with the help of high resolution CFD simulations, and second, to develop a Horizontal Axis Tidal Turbine (HATT) simulation system that could implement the impacts of tidal stream turbines on surface waves with a realistic spatial scale.

This paper details one high resolution CFD model for tidal turbine impact assessment on surface waves. Understandings obtained from the CFD modelling then advise turbine parameterization in large scale oceanographic models. The high resolution modelling is based on a CFD solver — ANSYS FLUENT. The implementation of effects of turbine operation on surface waves is an extension of the turbine simulation platform reported in [26], which parameterized tidal turbines in the current and turbulence closure modules of FVCOM. Impacts of tidal turbines on surface waves are considered in this new model by modification of wave energy flux across the device. A thorough validation study is also presented in which the turbine representation and operation in the CFD models is validated against laboratory data collected from an experiment conducted at the University of Hull using their 'Environment Simulator Laboratory Flume' [5] and the FVCOM model is verified utilizing the CFD simulated results.

The structure of the paper is provided as follows for clarity. Firstly in Section 2 ANSYS FLUENT and the FVCOM model are introduced. The integration of turbine simulation within these two frameworks is also discussed in this section. Next, Section 3 introduces the exploratory CFD models which aim to reveal the impacts of turbines on surface waves. A set of experimental data was used for CFD model validation in this section. Section 4 details the verification study for the turbine implementation in FVCOM which considers surface waves. Note that as the experimental data available was considered insufficient for comprehensive validation, verification in this section is based on data generated via the CFD modelling detailed in Section 3. In Section 5, the turbine simulation system developed based on FVCOM is applied to test cases in order to reveal impacts of a standalone turbine on its surroundings which incorporate wave-current interaction processes. A set of discussion is presented in Section 6, followed by concluding remarks given in Section 7 to summarise important results from sections 4 and 5, along with suggestions for potential future developments.

2. Modelling system

2.1. ANSYS FLUENT — a CFD solver

FLUENT solves the three-dimensional Reynolds-averaged Navier-Stokes (RANS) equations which can be written in tensor form as follows:

$$\frac{\partial \rho}{\partial t} + \frac{\partial \rho \bar{u}_i}{\partial x_i} = 0 \quad (1)$$

$$\frac{\partial(\rho\bar{u}_i)}{\partial t}+\frac{\partial(\rho\bar{u}_i\bar{u}_j)}{\partial x_j} = -\frac{\partial \bar{P}}{\partial x_i}+\frac{\partial}{\partial x_j}[\mu(\frac{\partial \bar{u}_i}{\partial x_j}+\frac{\partial \bar{u}_j}{\partial x_i})-\frac{2}{3}\mu\frac{\partial u_j}{\partial x_i}\delta_{ij}]+\frac{\partial}{\partial x_j}(-\rho\overline{u_i' u_j'})+F_i \quad (2)$$

where ρ is the water density; t is time; μ is the molecular viscosity; δ_{ij} is the Kronecker delta and F_i are external body forces in the i directions (x, y, z). $\bar{u}_i$ $(\bar{u}, \bar{v}, \bar{w})$ and u_i' (u', v', w') are the time-averaged (mean) and fluctuating water velocities in the x_i (x, y, z) directions, respectively. The combination of these two velocity components forms the instantaneous (exact) velocities:

$$u_i = \bar{u}_i + u_i' \quad (3)$$

Likewise, $\bar{P}$ is the time-averaged static pressure and for all scalar variables:

$$\phi = \bar{\phi} + \phi' \quad (4)$$

where ϕ denotes a scalar quantity such as pressure and $\bar{\phi}$ and ϕ' are the mean and fluctuating components of a scalar variable.

The Reynolds stress terms, $-\rho\overline{u_i{}'u_j{}'}$, which appear on the right hand side of Equation 2 represent the effects of turbulence and are modelled based on the Shear Stress Transport (SST) $k-\omega$ turbulence closure [38] in this research.

To simulate the wind-wave-induced free surface effects, the Volume of Fluid (VOF) method is used in FLUENT. The formulation of the VOF model relies on the fact that the modelled phases are not immiscible. It calculates the fractions (α_i, $0 < \alpha_i < 1$) of the simulated phases (water and air in the present research) in each computational cell and in each control volume. The volume fractions of all phases sum to unity. Based on the local value of α_i, the appropriate properties and variables will be assigned to each control volume within the domain.

A single momentum equation which is dependent on the volume fractions of all phases through the properties ρ and μ is solved throughout the calculation domain, and the computed velocity field is shared among the phases. The momentum equation is given by

$$\frac{\partial}{\partial t}(\rho\vec{v}) + \bigtriangledown\cdot(\rho\vec{v}\vec{v}) = -\bigtriangledown p + \bigtriangledown\cdot\left[\mu(\bigtriangledown\vec{v} + \bigtriangledown\vec{v}^T)\right] + \rho\vec{g} + \vec{F} \tag{5}$$

where ρ is the volume-fraction-averaged density $\rho = \sum \alpha_i\rho_i$ and μ the volume-fraction-averaged viscosity calculated in the same manner.

A continuity equation for the volume fraction of one (or more) of the phases helps to track the interface(s) between the phases. For the i^{th} phase, this equation takes the form of the following:

$$\frac{\partial \alpha_i}{\partial t} + \vec{v} \cdot \bigtriangledown \alpha_i = 0 \quad (6)$$

Additional scalar equations, such as those solving turbulence quantities, are also processed applying the shared-fields approach; i.e. only a single/a single set of transport equations is solved and the variables (e.g., k and ω) are shared by the phases throughout the domain.

A wave boundary condition is applied to the velocity inlet of the VOF model to enable the simulation of wave propagation. FLUENT provides a good variety of wave theories such as first order linear wave theory and second/higher order Stokes wave theories. The choice of wave theory is made based on Ursell number ($U_r = \frac{HL^2}{d^3}$) and wave steepness (H/L), where H, L and d are wave height, wave length and water depth, respectively. Linear wave theory is suitable when $U_r < 40$, given $H/L < 0.04$ and second/higher order Stokes wave theories are more appropriate when $U_r < 40$ and $H/L > 0.04$ [39]. The wave theories are fully coupled with the continuity and momentum equations of FLUENT. Details of the wave theories and the wave-current coupling can be found in [38, 40].

2.2. Representation of HATT in FLUENT

The Virtual Blade Model (VBM) is adopted in this research to simulate HATT in FLUENT. In VBM, the actual blades are not directly present. Instead, the rotor is simulated inside a rotor disk fluid zone across which the virtual blades swipe. The virtual blades are achieved through adding a body force in the x, y and z directions. This method is an application of a built-in blade simulating scheme — Blade Element Method (BEM) — within ANSYS

FLUENT. In BEM, each blade is divided into small sections from root to tip. The lift and drag forces exerted on each segment are calculated based on the blade design as well as the lift and drag coefficients of each section:

$$f_{L,D} = c_{L,D} \cdot c(r/R) \cdot \frac{\rho \cdot V_{tot}^2}{2} \tag{7}$$

where $c_{L,D}$ is lift/drag coefficient specified by the user; $c(r/R)$ is the chord length; ρ is the fluid density and V_{tot} is the fluid velocity relative to the blade.

The lift and drag forces are then averaged over a full turbine rotation to calculate the force on each cell in the discretized domain:

$$F_{L,D_{cell}} = N_b \cdot \frac{dr \cdot d\theta}{2\pi} \cdot f_{L,D} \tag{8}$$

$$\vec{S}_{cell} = -\frac{\vec{F}_{cell}}{V_{cell}} \tag{9}$$

where N_b is the number of blades and V_{cell} is the volume of a grid cell.

2.3. Three-dimensional FVCOM

To model the impacts of tidal stream energy devices on coastal regions, FVCOM, which is a three-dimensional, free surface, terrain-following oceanographic model [14], is used in this research. The momentum and continuity equations of FVCOM are presented in Equations 10-13. FVCOM includes fully coupled wave-current-sediment modules and, therefore, is particularly useful for modelling coastal processes. Also, it uses an unstructured triangular mesh to discretize computational domains horizontally, which allows for high resolution around individual turbines whilst maintaining a smooth transition to a relatively large mesh size far from the turbines. Such a treatment of spatial discretization provides a good balance between accuracy and computational effort.

$$\frac{\partial u}{\partial t}+u\frac{\partial u}{\partial x}+v\frac{\partial u}{\partial y}+w\frac{\partial u}{\partial z}-fv=-\frac{1}{\rho}\frac{\partial(P_H+P_a)}{\partial x}-\frac{1}{\rho}\frac{\partial q}{\partial x}+\frac{\partial}{\partial z}(K_m\frac{\partial u}{\partial z})+F_u \quad (10)$$

$$\frac{\partial v}{\partial t}+u\frac{\partial v}{\partial x}+v\frac{\partial v}{\partial y}+w\frac{\partial v}{\partial z}+fu=-\frac{1}{\rho}\frac{\partial(P_H+P_a)}{\partial x}-\frac{1}{\rho}\frac{\partial q}{\partial y}+\frac{\partial}{\partial z}(K_m\frac{\partial v}{\partial z})+F_v \quad (11)$$

$$\frac{\partial w}{\partial t}+u\frac{\partial w}{\partial x}+v\frac{\partial w}{\partial y}+w\frac{\partial w}{\partial z}=-\frac{1}{\rho}\frac{\partial q}{\partial z}+\frac{\partial}{\partial z}(K_m\frac{\partial w}{\partial z}) \quad (12)$$

$$\frac{\partial u}{\partial x}+\frac{\partial v}{\partial y}+\frac{\partial w}{\partial z}=0 \quad (13)$$

where x, y, and z are the east, north, and vertical axes in the Cartesian coordinate system; u, v, and w are the three velocity components in the x, y, and z directions respectively; P_a is the air pressure at sea surface; P_H is the hydrostatic pressure; q is the non-hydrostatic pressure; f is the Coriolis parameter and K_m is the vertical eddy viscosity coefficient. F_u, F_v represent horizontal momentum terms.

Extensive work has been done by the authors to enable the prediction of complete three-dimensional velocity profiles and mixing in the wake of turbines by making modifications to the current and turbulence closure modules of FVCOM [26]. The current research further extends the turbine simulation platform reported in [26] in terms of proposing a way to incorporate the effects of turbines on surface waves in the model.

For completeness, the basic theory surrounding surface waves and wave-current coupling in FVCOM is given as follows. More details of the model can be found in [41].

To simulate surface wave propagation, Simulating Waves Nearshore (SWAN) [42] is integrated with FVCOM. The governing equation of the wave action density spectrum is given as:

$$\frac{\partial N}{\partial t} + \bigtriangledown \cdot \left[\left(\vec{C}_g + \vec{V} \right) N \right] + \frac{\partial C_\sigma N}{\partial \sigma} + \frac{\partial C_\theta N}{\partial \theta} = \frac{S_{tot}}{\sigma} \tag{14}$$

where N is the wave action density spectrum, $\vec{C}_g$ is the group velocity vector, $\vec{V}$ is the ambient water current vector, σ is the relative frequency, θ is the wave direction, C_σ and C_θ are the wave propagation velocities in the frequency domain and directional space respectively and S_{tot} is the source-sink term considering wind-induced wave growth, nonlinear transfer of wave energy due to three-wave interactions, nonlinear transfer of wave energy due to four-wave interactions, wave decay due to white capping, wave decay due to bottom friction and wave decay due to depth-induced wave breaking. More details are available in the SWAN technical manual [42].

Due to the presence of surface waves, the bottom boundary layer is affected and the shear stress is much higher than that due to current alone [35]. To take this into account, a special treatment is needed close to the bed, which is implemented in the bottom boundary layer module (BBL). BBL calculates the bottom shear stresses under the condition of combined waves and currents. The calculation of bottom shear stress is important as it influences the flow field as well as sediment transport patterns. The BBL module developed by [43] based on the theory proposed by [44] was converted into an unstructured-grid finite-volume version and implemented in FVCOM. It is, hence, used in the present research. Details of BBL can be found in [43].

FVCOM includes a wave-current-sediment fully coupled system. After initialization, the wave module starts to solve the wave dynamics, providing information of surface waves. The interactions between the current and wave modules are achieved through radiation stress terms according to Mellor's theory [45, 46, 47]. Results from the current module, velocities and surface elevation in particular, provide the wave module feedback for the next time step calculation. Results from the current and wave modules are then sent to the BBL module to calculate the bottom stresses under the combined influence of waves and current. These stresses are then used to solve the momentum equations.

2.4. Representation of HATT in FVCOM

As will be demonstrated by CFD experiments in Section 3, surface wave height is affected by the inclusion of turbines. To represent this effect, one of the built-in features of SWAN — "OBSTACLE" is applied in the present study. The OBSTACLE routine absorbs wave energy along a finite line (defined between two locations) and dissipates it according to a constant transmission coefficient K_t. A detailed implementation of the OBSTACLE routine in this context can be found in [48].

To model the effect of turbines on waves, the OBSTACLE energy absorption line length in the model is set to the diameter of the simulated turbine. Note however that the impact of the line length upon the simulation is not continuous, as it absorbs energy only where it intersects with the mesh. In other words, two energy absorption lines of different length but with ends lying in the same respective triangle segments would have equal effect. The line is positioned in a way that it passes through the centre and crosses two sides of the triangles selected to house the turbine (see Figure 1). It should be pointed out that the turbine parameterization in the current and turbulence closure modules of FVCOM reported in [26] are utilized in this research

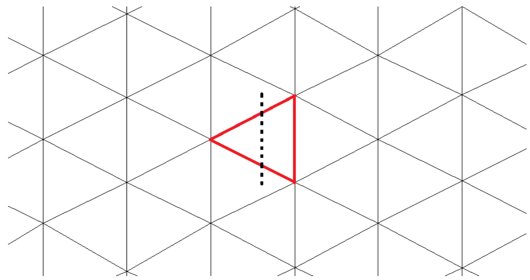

Figure 1: Illustration of the turbine position in the x-y plane on the mesh. The red triangle indicates the mesh element in which the turbine is implemented. The black dotted line illustrates the application of OBSTACLE.

when a turbine is present.

3. The CFD model

A CFD model is built in this research to study the impacts of tidal turbines on surface waves. It is based on an experiment carried out at the University of Hull using their ‘Environment Simulator Laboratory Flume’ [5]. The flume is 11 m in length, 1.6 m wide and 0.8 m deep. The water depth was 0.6m throughout the experiment. The flow rate at the inlet was 0.3 m/s. A surface wave propagating in the direction of the flow was imposed upon the inlet. The wave height and wave period were 0.15 m and 1 s, respectively. A horizontal axis rotor with a diameter of 0.2 m was located 0.2 m above the bed and the tip speed ratio (TSR) of the rotor was constantly 5.5. Measurements of velocity were taken along the centreline from 1D to 4D downstream of the rotor (where D is the turbine diameter).

Although a wide range of data was collected, the measurements did not include free surface variations which are the main focus of this research. Therefore, a CFD model replicating the experimental conditions was set up to capture the impacts of the rotor on surface waves. The CFD model was validated by recreating the conditions of the experiments for which measurements were available.

In the CFD model, the flume length was, instead of 11m, 3.1 m for ease of simulation. The velocity at the inlet was 0.3 m/s. A following wave with wave height of 0.15 m and wave period of 1 s was imposed at the inlet. The computation of wave propagation is based on the 2nd-order wave theory. To reduce the wave energy being reflected back into the flume from the exit, three porous zones, with thickness of 0.2m, 0.2m and 0.1m, were set at the outlet boundary, with porosity declining from 0.95 to 0.9 to 0.8. Essential configurations of VBM, i.e. geometrical setup and running parameters of the rotor are specified according to [49].

Figure 2 compares the ensemble average of stream-wise flow velocity profiles predicted by the CFD model against that measured in the laboratory at 1D, 2D, 3D and 4D downstream of the rotor. It should be noted that there are overlaps in the measured profiles. This is because in the laboratory, the centreline slice on which the velocities were measured was divided into 9 sub-slices and each of these sub-slices overlaps with its neighbour sub-slices. The overlaps provide a way to ensure the sub-slices are aligned correctly.

It can be seen from Figure 2 that the computed velocity profiles at all 4 locations agree well with the measurements at the rotor swiping layers with the exception of location 1D specifically above the rotor hub. This is due to the fact that the rotor housing and supporting structure (suspending the turbine from above) in the laboratory flume interfere with the flow at 1D. As these additional structures are not accounted for in the model, the result

Table 1: NSME for the CFD case against the experimental data

1D	2D	3D	4D
0.88	0.93	0.91	0.91

differs in this area. Further, the velocities in the region below the rotor are over-estimates. This over-estimation is likely due to a slightly over-predicted near bed wave boundary layer effect. To quantify the agreement between the predictions and measurements, the Nash Sutcliffe Model Efficiency (NSME) is calculated based on Equation 15 for each location for the rotor swiping layers and provided in Table 1. The NSME has been widely used to quantify the accuracy of model prediction, and the model performance is considered as excellent for NSME in between 0.65-1, very good for 0.65-0.5, good for 0.5-0.2, and poor for less than 0.2 (e.g. [50, 51, 52]). Therefore, the agreement between FLUENT based CFD model results and measured data are considered to be satisfactory at all sites.

$$NSME = 1 - \frac{\sum_{i=1}^{n}(q_i - q_{iest})^2}{\sum_{i=1}^{n}(q_i - \bar{q})^2} \qquad (15)$$

where n is the number of records in the validation data; q_i is the validation data; q_{iest} is the calculated result; $\bar{q}$ is the average of the validation data.

After being validated, the CFD model predicted free surfaces are studied to investigate the impacts of tidal turbines on surface waves. For this purpose, an undisturbed case (i.e. no turbine) was run to provide baseline surface wave profiles. The computed free surfaces at the two time instants when the trough and peak pass the turbine location are presented in Figure 3 (A) and 3 (B) respectively. It can be seen from Figure 3 that the inclusion of the

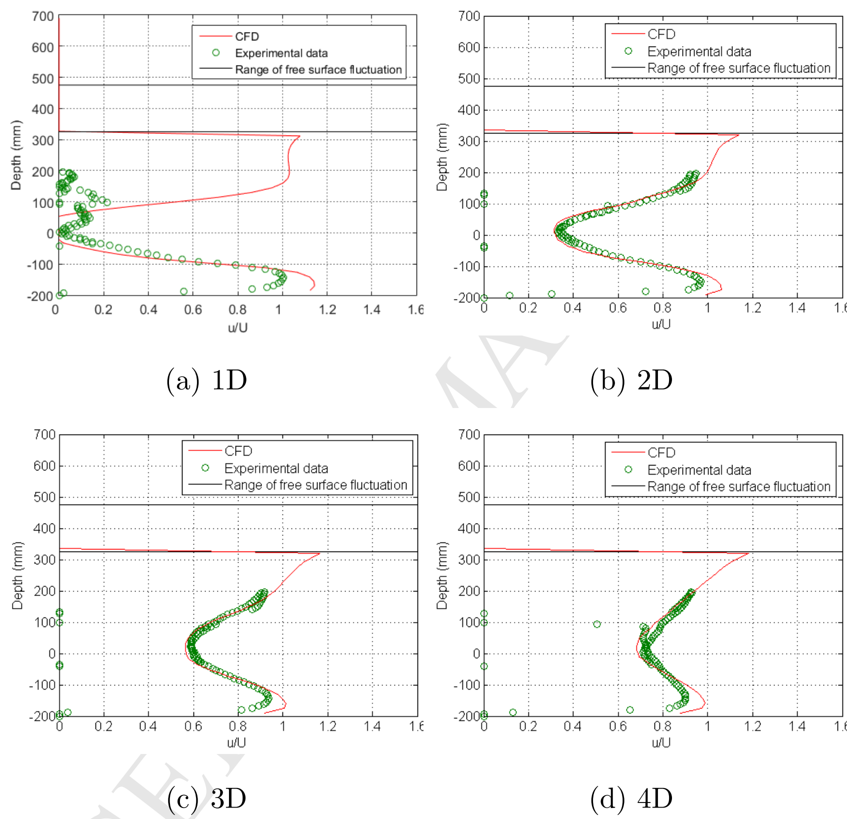

Figure 2: Normalized velocity profiles of the wave-current CFD case against those measured in the laboratory at 1D, 2D, 3D and 4D downstream of the rotor.

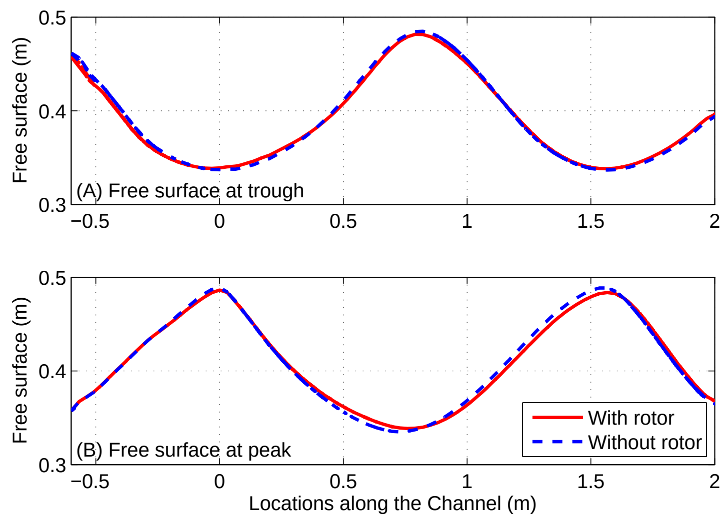

Figure 3: CFD predicted free surfaces at the wave trough (A) and peak (B) with and without the rotor. The rotor is positioned at 0 m along the channel.

rotor reduces the wave height; The wave height drops by $\sim 2.5\%$ when the rotor is present. It is also observed from Figure 3 that the wave length is increased due to the inclusion of the rotor.

The deformation of surface waves observed above, i.e. wave height drop and wave length increase, is likely to be caused by wave-current interactions. The obstruction effect of the rotor in motion forces the passing water to flow around the device, causing the velocity near the free surface to be increased. The accelerated flow at the surface results in a faster transport of wave energy and, consequently, reduced wave height and increased wave length.

4. Verification of the FVCOM model

This section explores the possibility of using the OBSTACLE mentioned above to represent the observed rotor-caused wave height drop. Hence, a

FVCOM based model was set up according to the above-mentioned experimental conditions. The mesh of the model has a uniform spatial resolution of 0.2 m (i.e. 1D) throughout the computational domain. Vertically, the water column is evenly divided into 50 sigma layers to accommodate the turbine representation in the current and turbulence modules recorded in [26].

The turbine effects on surface wave propagation is represented by subtracting a certain amount of energy from the energy conservation equation (Equation 14) as discussed in Section 2.4. In particular, the wave energy transmission coefficient K_t needs to be estimated. For this purpose, three cases are tested: baseline case where turbine is absent and the hydrodynamics resemble those of the undisturbed experimental conditions, case TNO where the turbine is present but OBSTACLE is deactivated, and case TYO where both the turbine and OBSTACLE are implemented. In case TYO, the wave energy transmission coefficient of OBSTACLE, K_t, is 0.98.

To verify the choice of K_t, Figure 4 compares the drop of wave height in percentage along the channel of the two FVCOM cases, TYO and TNO, and that of one of the CFD models (rotor positioned at 0.2 m above the bed). Wave height drop in percentage (hereafter wave height drop) is defined as the ratio between the decrease in wave height and the background wave height. It is obvious that the wave height drop at the turbine location predicted by TNO is $\sim 1.0\%$ less than that predicted by the corresponding CFD case. This difference is quite significant given that the correct drop is $\sim 2.5\%$ at the turbine location. The result of case TYO shows that the wave height drop is increased to the correct level by activating OBSTACLE; it is increased by $\sim 0.9\%$ at the turbine location due to the introduction of OBSTACLE. Hence,

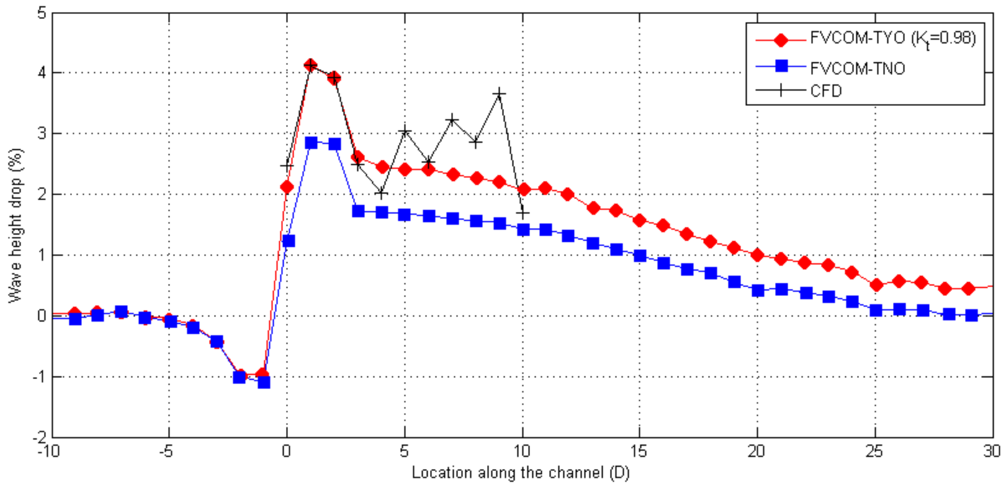

Figure 4: Wave height drop in terms of percentage along the channel for two FVCOM cases, TYO and TNO, and for the wave-current CFD case (the turbine is positioned at 0D).

the built-in feature OBSTACLE provides an effective way to simulate the turbine-caused wave height reduction.

The consistency between the CFD and FVCOM simulated wave heights in the wake of the turbine is obtained through calibrating the wave energy transmission coefficient K_t mentioned in Section 2.4 according to the results of the CFD model. However, it should be noted that the two models are based on different wave theories: the CFD model uses linear wave theory while the wave model in FVCOM (i.e. SWAN) is a spectral wave model. The reason the above-mentioned match is achievable despite different wave theories are applied is that the action balance equation of SWAN (Equation 14) is in fact an energy transfer equation derived based on the linear wave theory used in the CFD model. The spectrum which contains information of wave energy in different directions and frequencies can be regarded as a superposition of independent waves following the linear wave theory.

5. Application —Standalone turbine tests

This section investigates the effects of the inclusion of waves and activation of OBSTACLE upon the bottom shear stress based on a series of tests carried out using a prototype 15 m diameter turbine model as the test bed [26]. Water depth of these cases is 45 m and the turbine hub is located at a depth of 22.5 m. The flow and wave conditions are set to reflect those of the Anglesey coast, North Wales, UK, which is identified as one of the potential locations for tidal energy exploitation [53]. The water velocity is 1.0 m/s. The significant wave height is 2.4 m and wave period is 7 s: typical conditions of storms observed along the Anglesey coast [54].

The results of a current-only case (case TbM (BBL)) and a wave-imposed case without OBSTACLE (case TNO15) are compared to reveal the impact of surface waves on bottom shear stress. Another wave-current coupled case with OBSTACLE activated (case TYO15) is also tested in this section to further discuss how OBSTACLE affects the prediction of bottom shear stress. Turbine simulation in the current and turbulence modules is activated in these cases according to [26]. Bottom shear stress of these three cases are calculated through the BBL module [41] mentioned above. In case TYO15, the OBSTACLE wave energy absorption line (Figure 1) is 15m long and K_t is 0.98.

The computed significant wave height of cases TYO15 and TNO15 are shown in Figure 5 (A). Figure 5 (B) & (C) show normalized water velocity at the surface and bottom shear stress for cases TYO15, TNO15 and TbM

(BBL). It is observed from Figure 5 (A) that the inclusion of the turbine is causing the significant wave height decrease by $\sim 4.7\%$ beyond 10D downstream of the turbine and the inclusion of OBSTACLE further reduces the significant wave height by 0.6%.

In Figure 5 (B), velocity at the surface increases due to the implementation of the turbine; In this case a peak increase of $\sim 23\%$ is observed for TYO15 1D downstream of the turbine. Further, velocity at the surface for TNO15 is $\sim 4\%$ higher than TbM (BBL). This is due to the Stokes drift caused by the waves [55]. Note that waves propagating in the same direction of the carrying current are reported to cause a reduction of the flow velocity near the surface [56]. The inclusion of OBSTACLE leads to a reduction in wave height and hence an increase in flow velocity near the surface. This leads to a surface velocity increase of $\sim 3\%$ for TYO15 over TNO15.

In Figure 5 (C), it is observed that the inclusion of surface waves increases bottom shear stress by an average of $\sim 7\%$ (for both TYO15 and TNO15) in the regions upstream of the turbine and >9D downstream of the turbine. Difference in bottom shear stress caused by the waves from the turbine within 9D downstream of the turbine is relatively small (compared to outside this region). The retarding force which represents the turbine operation is playing the major role within this region, increasing the bottom shear stress by $\sim 50\%$ of all three cases. This is a result of the flow acceleration near the bed being identified by a three-dimensional model [26]. Also, the wave bottom boundary layer is likely to be dissipated by the strong mixing caused by the turbine. In the far wake region, as expected, the inclusion of OBSTACLE slightly reduces bottom shear stress compared to TNO15 ($\sim 2\%$ reduction).

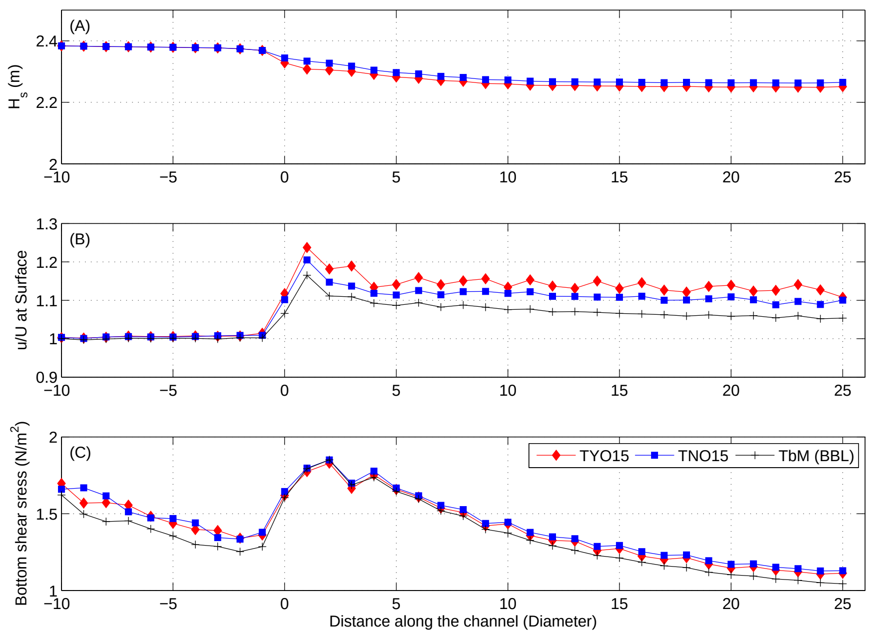

Figure 5: (A) Significant wave height (B) Normalized water velocity at the surface and (C) Bottom shear stress, all calculated under three different scenarios: TYO15 - Retarding force + turbulent terms + waves + obstacle, TNO15 - Retarding force + turbulent terms + waves and TbM (BBL) - Retarding force + turbulent terms with bottom shear stress calculated through BBL. (The turbine is positioned at 0D)

6. Discussions

6.1. Choice of turbine simulation method in FLUENT

Apart from VBM, there are a number of other methods that are widely used to model tidal turbines in CFD simulations, such as the Actuator Disc Method (ADM) which provides a momentum sink in the rotor disk fluid zone without the BEM [57], and the Moving Reference Frame (MRF) method which explicitly simulate the structure and the rotational motion of the turbine [58]. Compared to the fully resolved MRF, VBM has two well-documented limitations: 1) The mechanical turbulence caused by the turbine blades in the form of tip and hub vortex and the blade trailing edge wake is not accounted for [59], leading to under-predicted turbulence level behind the turbine [26]. 2) The lift and drag forces are annularly averaged over a full rotation circle, hence the VBM does not account for transient flow characteristics [10]. This could result in skipping of wave loadings on turbines due to the fact that waves can have higher frequencies than the blade passing frequency. Further, large shear can exist across the rotor depending on the vertical flow structure (especially when waves are present as the effect of waves vary significantly with depth), suggesting that the annularly averaged forces could be potentially invalid and a full multi-blade simulation is required to resolve the loadings more realistically. These disadvantages of VBM can result in fallacious power and fatigue analysis, which can ultimately lead to inaccurate prediction of design, build and maintenance costs [33]. However, considering that the main focus of this research is the impact of turbines on waves, instead of waves on the performance of turbines, and that the coefficients of VBM can be calibrated against measured data to ensure acceptable predicted flow conditions in the wake (e.g. [11, 26]), VBM is a viable choice for the purpose of this research. It is also worth noting that the integration of surface waves in CFD simulations can significantly increase the computational effort required, hence VBM which is comparably less computationally demanding can serve as a more feasible choice for wave-current simulations, especially in cases where multiple devices are presented.

6.2. Effect of static turbine simulation coefficients

By using VBM to simulate turbines, the lift/drag coefficients ($c_{L,D}$) of the turbine in the CFD simulations are assumed to be static despite the flow conditions. This could be incorrect as surface waves can cause time-varying loadings on turbines which in turn lead to time-dependent effective $c_{L,D}$ [33]. In terms of impact assessment, the fixed $c_{L,D}$ used in the CFD simulations could lead to under-/over-estimated instantaneous flow deceleration, turbulence generation, wave height modulation and bottom bed shear change. Similarly, the coefficients related to turbine simulation in FVCOM (those in current and turbulent mixing modules [26], as well as K_t in the wave module mentioned above) are static. Hence, the FVCOM model could also lead to the above-mentioned inaccurate instantaneous predictions. However, it is worth noting that the assessment of turbine-driven local/regional morphological evolution, which depend highly on the above-mentioned hydrodynamic factors, should take into consideration the life span of tidal turbine arrays which could be up to 100 years [60]. Therefore, the mean overall morphological evolution when considered over such a long time scale could become insensitive to the individual predictions.

7. Conclusions

The impact of turbines on surface waves is investigated in this study in light of the importance of surface waves on local/regional geomorphology and also as a response to the lack of attention on turbine-induced wave dynamic alternation in the literature. A CFD simulation with a turbine (blockage ratio 3.3% and TSR 5.5) located 0.4 m from the free surface revealed a $\sim 3\%$ reduction in wave height as well as a slight increase in wave length. To simulate the wave height drop in FVCOM, the OBSTACLE energy dissipation routine of the wave module (SWAN) was activated, and it captured the behaviour to a large extent (Figure 4). However, there are two obvious shortcomings with the modelling method. First, by simply using OBSTACLE which subtracts energy from the propagating surface waves, the model does not fully resolve the mechanism of turbine-wave interaction. In this regard, further work is recommended into the investigation of how turbines and surface waves interact. Second, only one turbine configuration is tested at a single depth. However, the specific value of K_t may in fact need to be defined as a function of depth which would also serve as an interesting avenue for investigation.

Impacts of tidal turbines on bed shear stress are also studied under wave-current fully coupled scenarios. It is found that although the inclusion of waves increased bed shear stress in the upstream area by an average of $\sim 7\%$, its influence on the bottom shear stress within the near wake zone, i.e. 0D-9D downstream of the turbine, is negligible. The turbine is the dominant factor within this region that increases the bottom shear stress by $\sim 50\%$, as the blockage effect of the turbine forces the water to flow around the device which increases the water velocity near the bed and subsequently increases the bottom shear stress. Impacts of waves on bottom shear stress resume in the far wake, i.e. >9D downstream of the turbine. The influence of OBSTACLE on bottom shear stress is also noticeable in the far wake. The OBSTACLE implemented in this work reduced bottom shear stress by $\sim 2\%$.

Acknowledgement

X. Li would like to acknowledge support from the Chinese Scholar Council and the University of Liverpool. Dr. Sufian also provided the settings for VBM in ANSYS FLUENT. The authors are grateful to Brendan Murphy for his help setting-up and running the experiments. The authors would also like to acknowledge funding from the Engineering and Physical Sciences Research Council (EPSRC) to grant EP/J010359/1 (Interactions of flow, tidal stream turbines and local sediment bed under combined waves and tidal conditions), which is part of the Supergen consortium.

[1] L. Myers, A. Bahaj, An experimental investigation simulating flow effects in first generation marine current energy converter arrays, Renewable Energy 37 (1) (2012) 28–36.

[2] L. Myers, A. Bahaj, Experimental analysis of the flow field around horizontal axis tidal turbines by use of scale mesh disk rotor simulators, Ocean Engineering 37 (2) (2010) 218–227.

[3] F. Maganga, G. Germain, J. King, G. Pinon, E. Rivoalen, Experimental characterisation of flow effects on marine current turbine behaviour and

on its wake properties, IET Renewable Power Generation 4 (6) (2010) 498–509.

[4] S. Tedds, I. Owen, R. Poole, Near-wake characteristics of a model horizontal axis tidal stream turbine, Renewable Energy 63 (2014) 222–235.

[5] L. B. Jordan, S. Simmons, S. McLelland, B. Murphy, D. Parsons, L. Vybulkova, The impact of tidal stream turbines on 3D flow and bed shear stress measured with particle image velocimetry in a laboratory flume, in: Proceedings of the 11th European Wave and Tidal Energy Conference, Nantes, France, 2015, pp. 654–660.

[6] A. Olczak, T. Stallard, P. Stansby, Tidal turbine wake recovery due to turbulent flow and opposing waves, Proceedings of the 2nd Oxford tidal energy workshop.

[7] X. Sun, J. Chick, I. Bryden, Laboratory-scale simulation of energy extraction from tidal currents, Renewable Energy 33 (6) (2008) 1267–1274.

[8] M. Harrison, W. Batten, L. Myers, A. Bahaj, Comparison between CFD simulations and experiments for predicting the far wake of horizontal axis tidal turbines, IET Renewable Power Generation 4 (6) (2010) 613–627.

[9] L. Bai, R. R. Spence, G. Dudziak, Investigation of the influence of array arrangement and spacing on tidal energy converter (TEC) performance using a 3-dimensional CFD model, in: Proceedings of the 8th European Wave and Tidal Energy Conference, Uppsala, Sweden, 2009, pp. 654–660.

[10] X. Bai, E. Avital, A. Munjiza, J. Williams, Numerical simulation of a marine current turbine in free surface flow, Renewable Energy 63 (2014) 715–723.

[11] R. Malki, I. Masters, A. J. Williams, T. N. Croft, Planning tidal stream turbine array layouts using a coupled blade element momentum–computational fluid dynamics model, Renewable Energy 63 (2014) 46–54.

[12] A. Goude, O. Ågren, Simulations of a vertical axis turbine in a channel, Renewable energy 63 (2014) 477–485.

[13] A. F. Shchepetkin, J. C. McWilliams, The regional oceanic modeling system (ROMS): a split-explicit, free-surface, topography-following-coordinate oceanic model, Ocean Modelling 9 (4) (2005) 347–404.

[14] C. Chen, H. Liu, R. C. Beardsley, An unstructured grid, finite-volume, three-dimensional, primitive equations ocean model: application to coastal ocean and estuaries, Journal of atmospheric and oceanic technology 20 (1) (2003) 159–186.

[15] I. G. Bryden, S. J. Couch, ME1 marine energy extraction: tidal resource analysis, Renewable Energy 31 (2) (2006) 133–139.

[16] R. Karsten, J. McMillan, M. Lickley, R. Haynes, Assessment of tidal current energy in the Minas Passage, Bay of Fundy, Proceedings of the Institution of Mechanical Engineers, Part A: Journal of Power and Energy 222 (5) (2008) 493–507.

[17] I. Walkington, R. Burrows, Modelling tidal stream power potential, Applied Ocean Research 31 (4) (2009) 239–245.

[18] Z. Defne, K. A. Haas, H. M. Fritz, Numerical modeling of tidal currents and the effects of power extraction on estuarine hydrodynamics along the Georgia coast, USA, Renewable Energy 36 (12) (2011) 3461–3471.

[19] R. Ahmadian, R. Falconer, B. Bockelmann-Evans, Far-field modelling of the hydro-environmental impact of tidal stream turbines, Renewable Energy 38 (1) (2012) 107–116.

[20] D. R. Plew, C. L. Stevens, Numerical modelling of the effect of turbines on currents in a tidal channel–Tory Channel, New Zealand, Renewable Energy 57 (2013) 269–282.

[21] D. Fallon, M. Hartnett, A. Olbert, S. Nash, The effects of array configuration on the hydro-environmental impacts of tidal turbines, Renewable Energy 64 (2014) 10–25.

[22] J. Thiébot, P. B. du Bois, S. Guillou, Numerical modeling of the effect of tidal stream turbines on the hydrodynamics and the sediment transport–Application to the Alderney Race (Raz Blanchard), France, Renewable Energy 75 (2015) 356–365.

[23] R. Martin-Short, J. Hill, S. Kramer, A. Avdis, P. Allison, M. Piggott, Tidal resource extraction in the Pentland Firth, UK: Potential impacts on flow regime and sediment transport in the Inner Sound of Stroma, Renewable Energy 76 (2015) 596–607.

[24] P. E. Robins, S. P. Neill, M. J. Lewis, Impact of tidal-stream arrays in relation to the natural variability of sedimentary processes, Renewable Energy 72 (2014) 311–321.

[25] T. Roc, D. C. Conley, D. Greaves, Methodology for tidal turbine representation in ocean circulation model, Renewable Energy 51 (2013) 448–464.

[26] X. Li, M. Li, S. J. McLelland, L.-B. Jordan, S. M. Simmons, L. O. Amoudry, R. Ramirez-Mendoza, P. D. Thorne, Modelling tidal stream turbines in a three-dimensional wave-current fully coupled oceanographic model, Renewable Energy 114 (2017) 297–307.

[27] G. McCann, Tidal current turbine fatigue loading sensitivity to waves and turbulence–a parametric study, in: Proceedings of the 7th European Wave and Tidal Energy Conference, Porto, Portugal, 2007.

[28] G. McCann, M. Thomson, S. Hitchcock, Implications of site-specific conditions on the prediction of loading and power performance of a tidal stream device, in: 2nd International Conference on Ocean Energy, Brest, France, 2008.

[29] C. Faudot, O. G. Dahlhaug, Prediction of wave loads on tidal turbine blades, Energy Procedia 20 (2012) 116–133.

[30] E. E. Lust, L. Luznik, K. A. Flack, J. M. Walker, M. C. Van Benthem, The influence of surface gravity waves on marine current turbine performance, International Journal of Marine Energy 3 (2013) 27–40.

[31] L. Luznik, K. A. Flack, E. E. Lust, K. Taylor, The effect of surface waves on the performance characteristics of a model tidal turbine, Renewable energy 58 (2013) 108–114.

[32] T. de Jesus Henriques, S. Tedds, A. Botsari, G. Najafian, T. Hedges, C. Sutcliffe, I. Owen, R. Poole, The effects of wave–current interaction on the performance of a model horizontal axis tidal turbine, International Journal of Marine Energy 8 (2014) 17–35.

[33] M. A. Holst, O. G. Dahlhaug, C. Faudot, Cfd analysis of wave-induced loads on tidal turbine blades, IEEE Journal of Oceanic Engineering 40 (3) (2015) 506–521.

[34] T. Spencer, I. Möller, F. Rupprecht, T. Bouma, B. Wesenbeeck, M. Kudella, M. Paul, K. Jensen, G. Wolters, M. Miranda-Lange, et al., Salt marsh surface survives true-to-scale simulated storm surges, Earth Surface Processes and Landforms 41 (4) (2016) 543–552.

[35] L. C. Van Rijn, L. C. van Rijn, L. C. van Rijn, Principles of sediment transport in rivers, estuaries and coastal seas, Vol. 1006, Aqua publications Amsterdam, 1993.

[36] M. S. Longuet-Higgins, Longshore currents generated by obliquely incident sea waves: 1, Journal of geophysical research 75 (33) (1970) 6778–6789.

[37] N. C. Kraus, S. Harikai, Numerical model of the shoreline change at oarai beach, Coastal Engineering 7 (1) (1983) 1–28.

[38] I. Fluent, Fluent users guide (2006).

[39] T. Hedges, Regions of validity of analytical wave theories, Oceanographic Literature Review 1 (43) (1996) 10.

[40] X. Li, 3D modelling of tidal stream energy extraction for impact assessment, Ph.D. thesis, School of Engineering, University of Liverpool (9 2016).

[41] C. Chen, G. Cowles, R. Beardsley, An unstructured grid, finite-volume coastal ocean model: FVCOM user manual, SMAST/UMASSD.

[42] N. Booij, R. Ris, L. H. Holthuijsen, A third-generation wave model for coastal regions: 1. model description and validation, Journal of Geophysical Research: Oceans (1978–2012) 104 (C4) (1999) 7649–7666.

[43] J. C. Warner, C. R. Sherwood, R. P. Signell, C. K. Harris, H. G. Arango, Development of a three-dimensional, regional, coupled wave, current, and sediment-transport model, Computers & Geosciences 34 (10) (2008) 1284–1306.

[44] O. S. Madsen, Spectral wave-current bottom boundary layer flows, Coastal Engineering Proceedings 1 (24).

[45] G. Mellor, The three-dimensional current and surface wave equations, Journal of Physical Oceanography 33 (9) (2003) 1978–1989.

[46] G. Mellor, Some consequences of the three-dimensional current and surface wave equations, Journal of Physical Oceanography 35 (11) (2005) 2291–2298.

[47] G. L. Mellor, M. A. Donelan, L.-Y. Oey, A surface wave model for coupling with numerical ocean circulation models, Journal of Atmospheric and Oceanic Technology 25 (10) (2008) 1785–1807.

[48] SWANTeam, SWAN Cycle III version 40.51 user manual, Delft University of Technology, Faculty of Civil Engineering and Geosciences, Environmental Fluid Mechanics Section (2006).

[49] S. Sufian, Numerical modeling of impacts from horizontal axis tidal turbines, Ph.D. thesis, School of Engineering, University of Liverpool (6 2016).

[50] D. Maréchal, A soil-based approach to rainfall-runoff modelling in ungauged catchments for england and wales.

[51] J. Allen, P. Somerfield, F. Gilbert, Quantifying uncertainty in high-resolution coupled hydrodynamic-ecosystem models, Journal of Marine Systems 64 (1-4) (2007) 3–14.

[52] L. Xiaorong, A. Plater, N. Leonardi, Modelling the transport and export of sediments in macrotidal estuaries with eroding salt marsh, Estuaries and Coasts (2018) 1–14.

[53] A. Iyer, S. Couch, G. Harrison, A. Wallace, Variability and phasing of tidal current energy around the United Kingdom, Renewable Energy 51 (2013) 343–357.

[54] M. Lewis, S. Neill, M. Hashemi, M. Reza, Realistic wave conditions and their influence on quantifying the tidal stream energy resource, Applied Energy 136 (2014) 495–508.

[55] K. E. Kenyon, Stokes drift for random gravity waves, Journal of Geophysical Research 74 (28) (1969) 6991–6994.

[56] M. Olabarrieta, R. Medina, S. Castanedo, Effects of wave–current interaction on the current profile, Coastal Engineering 57 (7) (2010) 643–655.

[57] L. Lavaroni, S. J. Watson, M. J. Cook, M. R. Dubal, A comparison of actuator disc and bem models in cfd simulations for the prediction of offshore wake losses, in: Journal of Physics: Conference Series, Vol. 524, IOP Publishing, 2014, p. 012148.

[58] T. ODoherty, A. Mason-Jones, D. ODoherty, C. Byrne, I. Owen, Y. Wang, Experimental and computational analysis of a model horizontal axis tidal turbine, in: 8th European Wave and Tidal Energy Conference (EWTEC), Uppsala, Sweden, 2009.

[59] T. Burton, D. Sharpe, N. Jenkins, E. Bossanyi, Wind energy handbook, John Wiley & Sons, 2001.

[60] S. Walker, R. Howell, P. Hodgson, A. Griffin, Tidal energy machines: A comparative life cycle assessment study, Proceedings of the Institution of Mechanical Engineers, Part M: Journal of Engineering for the Maritime Environment 229 (2) (2015) 124–140.

Impact of tidal stream energy device on surface wave dynamics are studied.

A 3D wave-current-sediment fully coupled large-scale numerical model is used.

Impact of turbines on surface waves are incorporated in the large-scale model.

Model prediction indicates a 3% turbine-caused drop in wave height.

Impact of the wave height drop on bed stress in the immediate wake is small.